Discontinuous Galerkin Computation of the Maxwell Eigenvalues on Simplicial Meshes

Annalisa Buffa

Istituto di Matematica Applicata e Tecnologie Informatiche - CNR, Via Ferrata 1, 27100 Pavia, Italy (email: annalisa@imati.cnr.it*)*

Paul Houston [1]

School of Mathematical Sciences, University of Nottingham, University Park, Nottingham, NG7 2RD, UK (email: Paul.Houston@nottingham.ac.uk*)*

Ilaria Perugia

Dipartimento di Matematica, Università di Pavia, Via Ferrata 1, 27100 Pavia, Italy (email: ilaria.perugia@unipv.it*)*

Abstract

This paper is concerned with the discontinuous Galerkin approximation of the Maxwell eigenproblem. After reviewing the theory developed in [5], we present a set of numerical experiments which both validate the theory, and provide further insight regarding the practical performance of discontinuous Galerkin methods, particularly in the case when non-conforming meshes, characterized by the presence of *hanging nodes*, are employed.

Key words: Discontinuous Galerkin methods, Maxwell's equations, discontinuous coefficients
PACS:

1 Introduction

In the recent article [5], a theory for the analysis of discontinuous Galerkin (DG) approximations to the Maxwell eigenproblem with discontinuous mate-

[1] Supported by the EPSRC (Grant GR/R76615).

rial coefficients was developed. In particular, this article identified necessary and sufficient conditions which the underlying DG method must satisfy in order to yield a spurious-free approximation. Moreover, a by-product of this spectral theory is a mathematical framework for the analysis of DG approximations of the indefinite source problem with discontinuous material coefficients; thereby, this theory generalizes the results obtained in [14] for the smooth material coefficient case.

In this paper, after reviewing the theoretical results of [5], we provide a thorough testing of DG approximations of the eigenproblem, in smooth and singular cases, with continuous and discontinuous coefficients, carried out with conforming and non-conforming meshes, with symmetric and non-symmetric DG methods. Interesting numerical studies of DG approximations are contained in [13] and [21]; the main goal there was to investigate the role of the penalty parameter appearing in the local discontinuous Galerkin method in terms of avoiding the pollution of the lowest part of the spectrum by eigenvalues related to the non-conformity of the approximation spaces, for a fixed mesh size. In contrast, the numerical results presented here are in the spirit of the *asymptotic* analysis of [5]. The aim of these experiments is to validate the theory of [5], and to provide further insight regarding the practical performance of DG methods for the numerical approximation of the Maxwell eigenproblem, particularly in the case when non-conforming meshes are employed.

Throughout this article, we denote by Ω the problem domain, which we assume to be a bounded Lipschitz polyhedral domain in $\mathbb{R}^d$, $d = 2, 3$, and by $\mathbf{n}$ the outward unit normal vector to its boundary $\partial\Omega$, pointing outside of Ω. For simplicity, we assume that $\partial\Omega$ is connected.

As model problem, we consider the following Maxwell eigenvalue problem with linear, inhomogeneous, anisotropic, and possibly discontinuous electric permittivity ε and magnetic permeability μ:

find $(\mathbf{0} \neq \mathbf{u}, \omega)$ such that

$$\nabla \times (\mu^{-1} \nabla \times \mathbf{u}) = \omega^2 \varepsilon \mathbf{u} \qquad \text{in } \Omega, \tag{1}$$

with $\mathbf{n} \times \mathbf{u} = \mathbf{0}$ on $\partial\Omega$ (notice that $\nabla \cdot (\varepsilon \mathbf{u}) = 0$).

In the rest of the paper, for a bounded domain D in $\mathbb{R}^d$, $d = 1, 2, 3$, we denote by $H^s(D)$ the standard Sobolev space of order $s \geq 0$ of real or complex valued functions, and by $\|\cdot\|_{s,D}$ the usual Sobolev norm. For $s = 0$, we write $L^2(D)$ in lieu of $H^0(D)$. We also use $\|\cdot\|_{s,D}$ to denote the norm for the space $H^s(D)^d$.

The paper is organized as follows: the continuous Maxwell problem and its DG discretisation are introduced in Section 2 and Section 3, respectively, and the main results obtained in [5] are reported in Section 4. Finally, Section 5 is

devoted to the presentation of numerical experiments.

2 Continuous Problem

If $d = 3$, we assume Ω is occupied by inhomogeneous, anisotropic materials, i.e., for which the electric permittivity $\varepsilon = \varepsilon(\mathbf{x})$ and magnetic permeability $\mu = \mu(\mathbf{x})$ are second order, real, symmetric, tensor-valued functions. We assume that there exists $\varepsilon^\star,\ \varepsilon_\star,\ \mu^\star,\ \mu_\star \in L^\infty(\Omega)$ such that

$$0 < \varepsilon_\star(\mathbf{x}) \leq \sum_{i,j=1}^{d} \varepsilon_{i,j}\xi_i\xi_j \leq \varepsilon^\star(\mathbf{x}) \qquad \text{a.e. in } \Omega\ \ \forall \xi \in \mathbb{R}^3,\ \|\xi\| = 1, \tag{2}$$

$$0 < \mu_\star(\mathbf{x}) \leq \sum_{i,j=1}^{d} \mu_{i,j}\xi_i\xi_j \leq \mu^\star(\mathbf{x}) \qquad \text{a.e. in } \Omega\ \ \forall \xi \in \mathbb{R}^3,\ \|\xi\| = 1. \tag{3}$$

If $d = 2$, $\varepsilon = \varepsilon(\mathbf{x})$ is again a second order, real, symmetric, tensor-valued function, whereas $\mu = \mu(\mathbf{x})$ is a scalar function. Therefore, the condition on ε is analogous to (2), and (3) becomes $0 < \mu_\star(\mathbf{x}) = \mu(\mathbf{x}) = \mu_\star(\mathbf{x})$.

Finally, we assume that there exists a partition of Ω into Lipschitz subdomains such that in each of them ε, μ, and μ^{-1} are smooth. A further restriction on the material coefficients will be stated in Section 3 below (see (6)).

We define, as usual, the following spaces of complex valued functions:

$$\begin{aligned}
&H_0(\mathrm{curl};\Omega) = \{\mathbf{v} \in L^2(\Omega)^d :\ \nabla \times \mathbf{v} \in L^2(\Omega)^{2d-3},\ \mathbf{n} \times \mathbf{v} = \mathbf{0} \text{ on } \partial\Omega\},\\
&H_0(\mathrm{curl}^0;\Omega) = \{\mathbf{v} \in H_0(\mathrm{curl};\Omega) :\ \nabla \times \mathbf{v} = \mathbf{0}\},\\
&H(\mathrm{div}^0_\varepsilon;\Omega) = \{\mathbf{v} \in L^2(\Omega)^d :\ \nabla \cdot (\varepsilon\mathbf{v}) = 0\},
\end{aligned}$$

and set $\mathbf{V} = H_0(\mathrm{curl};\Omega)$, $\mathbf{V}^0 = H_0(\mathrm{curl}^0;\Omega)$, and $\mathbf{W} = \mathbf{V} \cap H(\mathrm{div}^0_\varepsilon;\Omega)$.

Moreover, we denote by $(\cdot,\cdot)$ the standard inner product in $L^2(\Omega)^d$ given by $(\mathbf{u},\mathbf{v}) = \int_\Omega \mathbf{u} \cdot \overline{\mathbf{v}}\, d\mathbf{x}$, and write $L^2_\varepsilon(\Omega)^d$ for the space $L^2(\Omega)^d$ endowed with the ε–weighted inner product $(\mathbf{u},\mathbf{v})_\varepsilon = \int_\Omega \varepsilon\mathbf{u} \cdot \overline{\mathbf{v}}\, d\mathbf{x}$. The L^2–norm and the L^2_ε–norm are clearly equivalent, due to the assumptions on ε.

We endow $\mathbf{V}$ with the seminorm $|\mathbf{v}|_{\mathbf{V}} = \|\mu^{-1/2}\nabla \times \mathbf{v}\|_{0,\Omega}$, inner product $(\mathbf{u},\mathbf{v})_{\mathbf{V}} = (\mu^{-1}\nabla \times \mathbf{u}, \nabla \times \mathbf{v}) + (\mathbf{u},\mathbf{v})_\varepsilon$, and norm $\|\mathbf{v}\|^2_{\mathbf{V}} = |\mathbf{v}|^2_{\mathbf{V}} + \|\varepsilon^{1/2}\mathbf{v}\|^2_{0,\Omega}$.

Define the (hermitian) bilinear forms $a : \mathbf{V} \times \mathbf{V} \to \mathbb{C}$ and $b : \mathbf{V} \times \mathbf{V} \to \mathbb{C}$ as

$$a(\mathbf{u}, \mathbf{v}) = (\mu^{-1} \nabla \times \mathbf{u}, \nabla \times \mathbf{v}),$$
$$b(\mathbf{u}, \mathbf{v}) = a(\mathbf{u}, \mathbf{v}) + (\mathbf{u}, \mathbf{v})_\varepsilon \equiv (\mathbf{u}, \mathbf{v})_{\mathbf{V}}.$$

The variational formulation of the eigenproblem (1) consists in finding $(\mathbf{0} \neq \mathbf{u}, \omega) \in \mathbf{W} \times \mathbb{C}$ such that

$$a(\mathbf{u}, \mathbf{v}) = \omega^2 (\mathbf{u}, \mathbf{v})_\varepsilon \qquad \forall \mathbf{v} \in \mathbf{W}. \tag{4}$$

A standard way to discretise problem (4) consists in neglecting the constraint $\mathbf{u} \in \mathbf{W}$ and adding a zero frequency eigenspace corresponding to the *infinite-dimensional* space $\mathbf{V}^0$, leading to the following variational problem:

Find $(\mathbf{0} \neq \mathbf{u}, \omega) \in \mathbf{V} \times \mathbb{C}$ such that

$$a(\mathbf{u}, \mathbf{v}) = \omega^2 (\mathbf{u}, \mathbf{v})_\varepsilon \qquad \forall \mathbf{v} \in \mathbf{V}. \tag{5}$$

Clearly, $\omega^2 = 0$ is an eigenvalue of problem (5) with associated eigenspace $\mathbf{V}^0$. Moreover, the eigenvalue $\omega^2 = 0$ is isolated and all the other eigenvalues are real, positive, isolated, form a sequence accumulating only at $+\infty$, and their associated eigenspaces are finite dimensional (see, e.g., [18, Section 4.7]).

We end this section with some more notation needed in the rest of this paper.

Define the solution operator $A : L^2(\Omega)^d \to \mathbf{V}$ as follows: given $\mathbf{f} \in L^2(\Omega)^d$, $A\mathbf{f}$ is the (unique) element of $\mathbf{V}$ which satisfies

$$b(A\mathbf{f}, \mathbf{v}) = (\mathbf{f}, \mathbf{v})_\varepsilon \qquad \forall \mathbf{v} \in \mathbf{V}.$$

We have that $A \in \mathcal{L}(L^2(\Omega)^d, \mathbf{V})$. Clearly, $(\mathbf{u}, \omega)$ is an eigenpair of problem (5) if and only if $(\mathbf{u}, \lambda = \frac{1}{\omega^2+1})$ is an eigenpair of A; thus $\lambda = 1$ is an isolated eigenvalue of A with infinite multiplicity and associated eigenspace $\mathbf{V}^0$. Finally, we denote by $\sigma(A)$ and $\rho(A)$ the spectrum and resolvent set (in the complex plane), respectively, of the solution operator A and, for any $z \in \rho(A)$, we define the resolvent operator $R_z(A) = (z - A)^{-1}$ from $\mathbf{V}$ to $\mathbf{V}$.

3 Discontinuous Galerkin Approximation: Definitions and Standard Properties

In this section we introduce the meshes, DG spaces, and bilinear forms, and the standard assumptions satisfied by the most common DG methods.

3.1 Meshes, DG Spaces, and Norms

Let $\mathcal{T}_h$ be a conformal, shape-regular partition of Ω into simplices $\{K\}$, where $h = \max_{K\in\mathcal{T}_h} h_K$, with $h_K = \mathrm{diam}(K)$. We assume $\mathcal{T}_h$ to be aligned with the possible discontinuities of ε and μ. We denote by $\mathcal{F}_h$ the set of all the faces (edges for $d = 2$) of elements in $\mathcal{T}_h$.

We define, for later use, the broken regular spaces

$$\begin{aligned} H^s(\mathcal{T}_h)^d &:= \{\mathbf{v} \in L^2(\Omega)^d : \mathbf{v}|_K \in H^s(K)^d \quad \forall K \in \mathcal{T}_h\}, \quad \text{for } s \geq 0, \\ H^r(\mathrm{curl}; \mathcal{T}_h) &= \{\mathbf{v} \in L^2(\Omega)^d : \varepsilon\mathbf{v}|_K \in H^r(K)^d, \\ &\qquad \mu^{-1}\nabla \times \mathbf{v}|_K \in H^r(K)^{2d-3} \quad \forall K \in \mathcal{T}_h\}, \quad \text{for } r > 0, \end{aligned}$$

endowed with the norms

$$\begin{aligned} \|\mathbf{v}\|^2_{H^s(\mathcal{T}_h)^d} &= \sum_{K\in\mathcal{T}_h} \|\mathbf{v}\|^2_{s,K}, \\ \|\mathbf{v}\|^2_{H^r(\mathrm{curl};\mathcal{T}_h)} &= \sum_{K\in\mathcal{T}_h} \left(\|\varepsilon^{1/2}\mathbf{v}\|^2_{r,K} + \|\mu^{-1/2}\nabla \times \mathbf{v}\|^2_{r,K}\right), \end{aligned}$$

respectively. For piecewise smooth vector-valued functions $\mathbf{v}$, on interior faces, we denote by $[\![\mathbf{v}]\!]_T$ and $\{\!\{\mathbf{v}\}\!\}$ the tangential jump and mean value of $\mathbf{v}$, respectively. On boundary faces, we set $[\![\mathbf{v}]\!]_T = \mathbf{n} \times \mathbf{v}$ and $\{\!\{\mathbf{v}\}\!\} = \mathbf{v}$.

In addition to the assumptions on the coefficients in Section 2, we suppose that there exists a constant $\overline{\mu} > 0$, independent of the mesh size, such that

$$\max_{\mathbf{x}\in K} \frac{\mu^\star(\mathbf{x})}{\mu_\star(\mathbf{x})} \leq \overline{\mu} \qquad \forall\, K \in \mathcal{T}_h. \tag{6}$$

For $\ell \geq 1$, we define the discontinuous finite element space of complex valued functions:

$$\mathbf{V}_h := \{\mathbf{v} \in L^2(\Omega)^d : \mathbf{v}|_K \in \mathcal{P}^\ell(K)^d \ \ \forall K \in \mathcal{T}_h\}, \tag{7}$$

where $\mathcal{P}^\ell(K)$ is the space of complex valued polynomials of total degree at most ℓ on K. We point out that all the results shown below also hold when the local space $\mathcal{P}^\ell(K)^d$ of full polynomials of degree ℓ in (7) are replaced by Nédélec's elements of the first type [19]. For the case of parallelepipeds, we refer to Remark 4.5 below.

We define the sum space $\mathbf{V}(h) = \mathbf{V} + \mathbf{V}_h$, and endow both $\mathbf{V}_h$ and $\mathbf{V}(h)$ with the seminorm and norm

$$\begin{aligned} |\mathbf{v}|^2_{\mathbf{V}(h)} &= \|\mu^{-1/2}\nabla_h \times \mathbf{v}\|^2_{0,\Omega} + \|\mathtt{h}^{-1/2}[\![\mathbf{v}]\!]_T\|^2_{0,\mathcal{F}_h}, \\ \|\mathbf{v}\|^2_{\mathbf{V}(h)} &= |\mathbf{v}|^2_{\mathbf{V}(h)} + \|\varepsilon^{1/2}\mathbf{v}\|^2_{0,\Omega}, \end{aligned}$$

respectively, where ∇_h denotes the elementwise application of the ∇ operator. Here, we have used the notation $\|\varphi\|^2_{0,\mathcal{F}_h} := \sum_{f\in\mathcal{F}_h}\|\varphi\|^2_{0,f}$; we also write $\int_{\mathcal{F}_h}\varphi\,ds := \sum_{f\in\mathcal{F}_h}\int_f\varphi\,ds$. The mesh function $\mathtt{h}\in L^\infty(\mathcal{F}_h)$ is defined by

$$\mathtt{h}(\mathbf{x}) := h_f\,\mathtt{m}(\mathbf{x}), \qquad \mathbf{x}\in f,\ f\in\mathcal{F}_h,$$

with $h_f = \mathrm{diam}(f)$. The function $\mathtt{m}\in L^\infty(\mathcal{F}_h)$ is defined as follows: if μ_K denotes the extension of $\mu_{|_K}$ up to ∂K, and $|\mu_K(\mathbf{x})|$ denotes the spectral norm of the tensor $\mu_K(\mathbf{x})$, then $\mathtt{m}(\mathbf{x}) = \min\{|\mu_{K^+}(\mathbf{x})|, |\mu_{K^-}(\mathbf{x})|\}$, if $\mathbf{x}$ is in the interior of $\partial K^+\cap\partial K^-$, and $\mathtt{m}(\mathbf{x}) = |\mu_K(\mathbf{x})|$, if $\mathbf{x}$ is in the interior of $\partial K\cap\partial\Omega$.

We define the following seminorms and norms, respectively: given σ, $0<\sigma<1/2$, we write

$$|\mathbf{v}|^2_{+,\sigma} = \sum_{K\in\mathcal{T}_h}\left(h_K^{2\sigma}M_K\|\mu^{-1}\nabla\times\mathbf{v}\|^2_{\sigma,K} + h_K^2M_K\|\nabla\times(\mu^{-1}\nabla\times\mathbf{v})\|^2_{0,K}\right),$$
$$\|\mathbf{v}\|^2_{+,\sigma} = \|\mathbf{v}\|^2_{\mathbf{V}(h)} + |\mathbf{v}|^2_{+,\sigma};$$

here, and in the following, M_K is defined by $M_K = \max_{\mathbf{x}\in\overline{K}}|\mu_K(\mathbf{x})|$.

The following best approximation result holds true. (see [5, Appendix]).

Proposition 3.1 *Let $s\ge 0$, $r>0$, and $0<\sigma<\min\{r,1/2\}$. For all $\mathbf{v}\in H^r(\mathrm{curl};\mathcal{T}_h)$, with $(\nabla_h\times(\mu^{-1}\nabla_h\times\mathbf{v}))\in H^s(\mathcal{T}_h)^d$, we have*

$$\inf_{\mathbf{v}_h\in\mathbf{V}_h}\|\mathbf{v}-\mathbf{v}_h\|_{+,\sigma}$$
$$\le Ch^{\min\{r,\ell,s+1\}}\left(\|\mathbf{v}\|_{H^r(\mathrm{curl};\mathcal{T}_h)} + \left(\sum_{K\in\mathcal{T}_h}M_K\|\nabla_h\times(\mu^{-1}\nabla_h\times\mathbf{v})\|^2_{s,K}\right)^{1/2}\right),$$

where the constant $C>0$ is independent of the mesh size.

3.2 DG Bilinear Forms

Let $a_h : \mathbf{V}_h\times\mathbf{V}_h\to\mathbb{C}$ be the DG bilinear form obtained by discretising $a:\mathbf{V}\times\mathbf{V}\to\mathbb{C}$ by any DG method, and define

$$b_h(\mathbf{u},\mathbf{v}) = a_h(\mathbf{u},\mathbf{v}) + (\mathbf{u},\mathbf{v})_\varepsilon \qquad \forall\mathbf{u},\mathbf{v}\in\mathbf{V}_h.$$

We restrict ourselves to DG methods which provide *consistent* discretisations to the coercive source problem: given $\mathbf{f}\in L^2(\Omega)^d$, find $\mathbf{u}\in\mathbf{V}$ such that

$$b(\mathbf{u},\mathbf{v}) = (\mathbf{f},\mathbf{v}) \quad \forall\,\mathbf{v}\in\mathbf{V}. \tag{8}$$

Thus, we are also requiring $a_h(\mathbf{u},\mathbf{v})$ to be well-defined for all the pairs $(\mathbf{u},\mathbf{v})$ such that $\mathbf{u}\in\mathbf{V}$ with $\nabla_h\times(\mu^{-1}\nabla_h\times\mathbf{u})\in L^2(\Omega)^d$, and $\mathbf{v}\in\mathbf{V}_h$.

To fix the ideas, we consider the interior penalty methods, for which

$$\begin{aligned} a_h(\mathbf{u},\mathbf{v}) =& (\mu^{-1}\nabla_h\times\mathbf{u},\nabla_h\times\mathbf{v}) - \int_{\mathcal{F}_h}[\![\overline{\mathbf{v}}]\!]_T\cdot\{\!\{\mu^{-1}\nabla_h\times\mathbf{u}\}\!\}\,ds \\ & - k\int_{\mathcal{F}_h}[\![\mathbf{u}]\!]_T\cdot\{\!\{\mu^{-1}\nabla_h\times\overline{\mathbf{v}}\}\!\}\,ds + \int_{\mathcal{F}_h}\mathtt{a}[\![\mathbf{u}]\!]_T\cdot[\![\overline{\mathbf{v}}]\!]_T\,ds, \end{aligned}$$

with

$$\mathtt{a} := a_{\mathrm{IP}}\mathtt{h}^{-1}, \tag{9}$$

$a_{\mathrm{IP}} > 0$ being a parameter independent of the mesh size and the material coefficients. Setting $k = 1, -1, 0$, gives rise to the symmetric interior penalty (SIP) method [2], the non-symmetric interior penalty (NIP) method [20], and the incomplete interior penalty (IIP) method [9], respectively. The local discontinuous Galerkin (LDG) method, as well as one of the variants of the IP and LDG methods (see [3] and the references therein), could also be considered instead.

Define the kernel of $a_h(\cdot,\cdot)$ and its $\mathbf{V}(h)$–orthogonal complement as follows:

$$\begin{aligned} K_h &= \{\mathbf{v}\in\mathbf{V}_h:\ a_h(\mathbf{v},\mathbf{w}) = 0\ \forall\mathbf{w}\in\mathbf{V}_h\}, \\ K_h^{\perp} &= \{\mathbf{v}\in\mathbf{V}_h:\ (\mathbf{v},\mathbf{w})_{\mathbf{V}(h)} = 0\ \forall\mathbf{w}\in K_h\}. \end{aligned}$$

Notice that, also for the non-hermitian NIP and IIP methods, the left kernel coincides with the right kernel, i.e., $a_h(\mathbf{v},\mathbf{w}) = 0$ for all $\mathbf{v}\in\mathbf{V}_h$ and $\mathbf{w}\in K_h$.

As in the continuous case, we define the DG solution operator $A_h : L^2(\Omega)^d \to \mathbf{V}_h$ as follows: given $\mathbf{f}\in L^2(\Omega)^d$, $A_h\mathbf{f}$ is the (unique) element of $\mathbf{V}_h$ which satisfies

$$b_h(A_h\mathbf{f},\mathbf{v}) = (\mathbf{f},\mathbf{v})_\varepsilon \qquad \forall\mathbf{v}\in\mathbf{V}_h.$$

The operator A_h is well-defined and $A_h\in\mathcal{L}(L^2(\Omega)^d,\mathbf{V}_h)$ (see Remark 3.3 below). Finally, we denote by $\sigma(A_h)$ and $\rho(A_h)$ the spectrum and the resolvent set, respectively, of the DG solution operator A_h and, for any $z\in\mathbb{C}$, we formally define the resolvent operator $R_z(A_h) = (z - A_h)^{-1}$ from $\mathbf{V}_h$ to $\mathbf{V}_h$.

For the considered DG bilinear forms, the following proposition holds (the first part is standard, while the second part has been proved in [5, Appendix]).

Proposition 3.2 (Coercivity in seminorm and continuity) *Provided that a_{IP} in (9) is large enough, in the case of the SIP and IIP methods, there exist positive constants α and γ, independent of the mesh size, such that*

$$\begin{aligned} &\mathrm{Re}\,[a_h(\mathbf{v},\mathbf{v})] \geq \alpha\,|\mathbf{v}|^2_{\mathbf{V}(h)} && \forall\mathbf{v}\in\mathbf{V}_h, \\ &|a_h(\mathbf{u},\mathbf{v})| \leq \gamma\|\mathbf{u}\|_{\mathbf{V}(h)}\|\mathbf{v}\|_{\mathbf{V}(h)} && \forall\mathbf{u},\mathbf{v}\in\mathbf{V}_h. \end{aligned}$$

Moreover, for any σ, such that $0 < \sigma < \min\{1/2, r\}$, there exists a constant

$\gamma_\sigma > 0$, *independent of the mesh size, such that*

$$|a_h(\mathbf{u},\mathbf{v})| \leq \gamma_\sigma \|\mathbf{u}\|_{+,\sigma}\|\mathbf{v}\|_{\mathbf{V}(h)}$$

for all $\mathbf{u} \in H^r(\mathrm{curl};\mathcal{T}_h)$ *with* $\nabla_h \times (\mu^{-1}\nabla_h \times \mathbf{u}) \in L^2(\Omega)^d$, *and* $\mathbf{v} \in \mathbf{V}_h$.

Remark 3.3 *From the coercivity property in Proposition 3.2 it follows that*

$$\mathrm{Re}\,[b_h(\mathbf{v},\mathbf{v})] \geq \min\{\alpha,1\}\|\mathbf{v}\|^2_{\mathbf{V}(h)} \qquad \forall \mathbf{v} \in \mathbf{V}_h.$$

Therefore, for any $\mathbf{f} \in L^2(\Omega)^d$, *there exists a unique* $\mathbf{u}_h \in \mathbf{V}_h$ *such that* $b_h(\mathbf{u}_h,\mathbf{v}) = (\mathbf{f},\mathbf{v})_\varepsilon$ *for all* $\mathbf{v} \in \mathbf{V}_h$, *and* $\|\mathbf{u}_h\|_{\mathbf{V}(h)} \leq C\|\mathbf{f}\|_{0,\Omega}$, *where* $C > 0$ *is independent of the mesh size.*

Finally, the following statement is a straightforward consequence of Proposition 3.2 (see Remark 3.3), consistency, and Proposition 3.1.

Corollary 3.4 (Convergence for the coercive problem) *Let* $\mathbf{u}$ *be the solution to the coercive source problem* (8) *with* $\mathbf{f} \in H(\mathrm{div}^0_\varepsilon;\Omega)$, *and let* $\mathbf{u}_h$ *be its DG approximation which satisfies* $b_h(\mathbf{u}_h,\mathbf{v}) = (\mathbf{f},\mathbf{v})_\varepsilon$ *for all* $\mathbf{v} \in \mathbf{V}_h$. *If* $\mathbf{u} \in H^r(\mathrm{curl};\mathcal{T}_h)$, $r > 0$ *(see [7]), and* $(\nabla_h \times (\mu^{-1}\nabla_h \times \mathbf{u})) \in H^s(\mathcal{T}_h)^d$, $s \geq 0$, *we have:*

$$\begin{aligned}&\|\mathbf{u}-\mathbf{u}_h\|_{\mathbf{V}(h)}\\ &\quad\leq Ch^{\min\{\ell,r,s+1\}}\left(\|\mathbf{u}\|_{H^r(\mathrm{curl};\mathcal{T}_h)} + \Big(\sum_{K\in\mathcal{T}_h} M_K\|\nabla\times(\mu^{-1}\nabla\times\mathbf{u})\|^2_{s,K}\Big)^{1/2}\right),\end{aligned}$$

where $C > 0$ *is independent of the mesh size.*

4 Theoretical Results

In this section we present the results of the theory developed in [5] for DG approximations of problem (5): find $(\mathbf{0} \neq \mathbf{u}_h, \omega_h) \in \mathbf{V}_h \times \mathbb{C}$ such that

$$a_h(\mathbf{u}_h,\mathbf{v}) = \omega_h^2(\mathbf{u}_h,\mathbf{v})_\varepsilon \qquad \forall \mathbf{v} \in \mathbf{V}_h. \tag{10}$$

4.1 Key Properties: Discrete Friedrichs Inequality and Gap Property

It has been established in [5] that the following two properties are sufficient for (10) to be *spurious-free*.

Property 1 (Discrete Friedrichs inequality) *There exists $C > 0$ independent of the mesh size such that*

$$\|\varepsilon^{1/2}\mathbf{v}\|_{0,\Omega}^2 \le C\,\mathrm{Re}\,[a_h(\mathbf{v},\mathbf{v})] \qquad \forall \mathbf{v} \in K_h^{\perp}.$$

Property 2 (Gap property) *For all h small enough, for any $\mathbf{w}_h \in K_h^{\perp}$ there exists $\mathbf{w} = \mathbf{w}(h) \in H(\mathrm{div}_{\varepsilon}^0;\Omega)$ such that*

$$\|\mathbf{w} - \mathbf{w}_h\|_{0,\Omega} \le \eta_h \|\mathbf{w}_h\|_{\mathbf{V}(h)}, \quad \textit{with } \eta_h \to 0 \textit{ as } h \to 0.$$

The DG methods considered in Section 3 actually satisfy Properties 1 and 2 (see again [5]). The proof of these results is based on an approximation property that allows us to find an $H_0(\mathrm{curl};\Omega)$–conforming finite element function close to any discontinuous one (see [16] and [14]), and on the *discrete compactness property* possessed by the conforming Nédélec elements of the second family (see, e.g., [6] or [4]). This is the reason why our analysis is restricted to the case of conforming meshes with no hanging-nodes.

In the next subsection we recall the main theoretical results which follow from Properties 1 and 2.

4.2 Spurious-Free Approximations

The main statement of this section is that the method (10) is *spurious-free* in the sense of [10] and [6] (see Theorem 4.2 below); this is a consequence of Proposition 3.2, Corollary 3.4, and Properties 1–2.

A key argument for the spectral correctness theory is the following theorem.

Theorem 4.1 *Fix $0 \neq z \in \rho(A)$. For h small enough, there exists a positive constant C only depending upon Ω and $|z|$ such that*

$$\|(z - A_h)\mathbf{f}\|_{\mathbf{V}(h)} \ge C\|\mathbf{f}\|_{\mathbf{V}(h)} \qquad \forall \mathbf{f} \in \mathbf{V}_h.$$

Theorem 4.1 implies that, for $0 \neq z \in \rho(A)$, the resolvent operator $R_z(A_h)$ introduced in Section 3.2 is a well-defined continuous operator from $\mathbf{V}_h$ to $\mathbf{V}_h$.

Let λ be an eigenvalue of A with algebraic multiplicity m, and let Γ be a circle in the complex plane centered at λ which lies in $\rho(A)$ and does not enclose any other point of $\sigma(A)$. According to [17, p. 178], we define the *spectral projections* E^{λ} and, for h small enough, E_h^{λ} from $\mathbf{V}_h$ into $\mathbf{V}(h)$ by

$$E^{\lambda} = \frac{1}{2\pi i}\int_{\Gamma} R_z(A)\,dz, \quad E_h^{\lambda} = \frac{1}{2\pi i}\int_{\Gamma} R_z(A_h)\,dz,$$

respectively. For h small enough, E_h^λ is well defined, owing to Theorem 4.1.

If Y and Z are closed subspaces of $\mathbf{V}(h)$, we set

$$\delta_h(\mathbf{x}, Y) := \inf_{\mathbf{y}\in Y} \|\mathbf{x}-\mathbf{y}\|_{\mathbf{V}(h)}, \qquad \delta_h(Y,Z) := \sup_{\substack{\mathbf{y}\in Y \\ \|\mathbf{y}\|_{\mathbf{V}(h)}=1}} \delta_h(\mathbf{y}, Z).$$

Theorem 4.2 *The method* (10) *is* spurious-free*, i.e., the following holds:*

i) Isolation of discrete essential spectrum: *If $\lambda_h \in \sigma(A_h)$, then $0 <$ Re $[\lambda_h] \leq 1$; $1 \in \sigma(A_h)$ and its associated eigenspace is K_h. Moreover, there exists $0 < \beta < 1$ independent of the mesh size such that, if $1 \neq \lambda_h \in \sigma(A_h)$,*

$$\text{Re } [\lambda_h] \leq \beta$$

(whenever $a_h(\cdot,\cdot)$ is hermitian, all the discrete eigenvalues are actually real).

ii) Non-pollution of the spectrum: *Let $G \subset \mathbb{C}$ be an open set containing $\sigma(A)$. Then, for h small enough, $\sigma(A_h) \subset G$.*

iii) Non-pollution of the eigenspaces: *For any $\lambda \in \sigma(A)$, we have*

$$\lim_{h\to 0} \delta_h(E_h^\lambda(\mathbf{V}_h), E^\lambda(\mathbf{V})) = 0.$$

iv) Completeness of the eigenspaces: *For any $1 \neq \lambda \in \sigma(A)$, we have*

$$\lim_{h\to 0} \delta_h(E^\lambda(\mathbf{V}), E_h^\lambda(\mathbf{V}_h)) = 0.$$

v) Completeness of the spectrum: *For any $\lambda \in \sigma(A)$, we have*

$$\lim_{h\to 0} \delta_h(\lambda, \sigma(A_h)) = 0.$$

Let $\lambda \neq 1$ be an eigenvalue of A with (finite) multiplicity m. The previous theorem guarantees that, for h small enough, there exist exactly m eigenvalues $\{\lambda_{1,h}, \ldots, \lambda_{m,h}\}$ of A_h (repeated with their multiplicities) such that

$$\lim_{h\to 0} \sup_{1\leq i\leq m} |\lambda - \lambda_{i,h}| = 0.$$

The convergence rates of this limit (convergence of eigenvalues) and of the one in Theorem 4.2 (convergence of eigenspaces) are given in the following theorem (its proof can be carried out as in [11]).

Theorem 4.3 *Let $\lambda \neq 1$ be in $\sigma(A)$. Then, for h small enough, it holds*

$$\begin{aligned} \delta_h(E^\lambda(\mathbf{V}), E_h^\lambda(\mathbf{V}_h)) &\leq C h^{\min\{\ell, \sigma_\lambda\}}, \\ \sup_{1\leq i\leq m} |\lambda - \lambda_{i,h}| &\leq C h^{\min\{\ell, \sigma_\lambda\}}, \end{aligned}$$

where σ_λ is the regularity exponent of $E^\lambda(\mathbf{V})$, i.e., $\mathbf{u} \in H^{\sigma_\lambda}(\mathrm{curl}; \mathcal{T}_h)$ for all $\mathbf{u} \in E^\lambda(\mathbf{V})$, and the constant C only depends on λ (and deteriorates for small values of λ). Moreover, for hermitian DG methods, we have

$$\sup_{1 \le i \le m} |\lambda - \lambda_{i,h}| \le C h^{2 \min\{\ell, \sigma_\lambda\}}.$$

Remark 4.4 *Properties 1 and 2 are not only sufficient but also necessary for* (10) *to be spurious-free (see [5, Section 5]).*

Remark 4.5 *On parallelepipeds/parallelograms, all the results in this section apply to the choice of $\mathbf{V}_h$ in (7) with the local Nédélec elements of the first type of degree ℓ, instead of the full polynomials of degree ℓ, whereas for the full polynomials of degree ℓ in each variable, namely the local Nédélec elements of the second type of degree ℓ, the obtained method can not be spurious-free (see [5, Proposition 7.13 and Remark 7.14]): this is confirmed by our numerical experiments (See Figure 2(b) in Section 5 below).*

5 Numerical Results

In this section we present a series of numerical experiments to highlight the practical performance of both the symmetric (SIP) and non-symmetric (NIP) interior penalty DG methods for the approximation of the eigenvalue problem (5). Results for the (non-symmetric) IIP method are not reported, for brevity, since they are completely analogous to the ones for the NIP method. For simplicity, we restrict ourselves to two-dimensional model problems; additionally, we note that throughout this section we select the constant appearing in the interior penalty stabilization function defined in (9) as follows: $a_{\mathrm{IP}} = 10\,\ell^2$, cf. [15], for example.

5.1 Example 1

In this first example we let $\Omega = (0, \pi)^2$ with $\varepsilon = I$ and $\mu = I$; thereby, the exact eigenvalues λ are given by $n^2 + m^2$, where n and m are positive integers. In this section, we investigate the asymptotic behaviour of the error in the approximation of the eigenvalue problem (5), based on employing both the SIP and NIP methods, on a sequence of successively finer triangular meshes for different values of the polynomial degree ℓ. For each method, we consider uniform conforming meshes, as well as 1– and 3–irregular meshes which contain hanging nodes; cf. Figure 1.

Firstly, however, in Figure 2 we show the lower part of the eigenspectrum

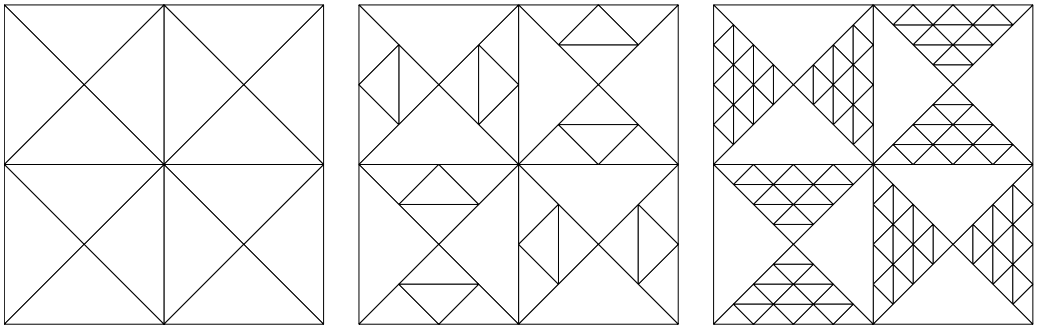

(a) (b) (c)

Figure 1. Example 1. Initial triangular meshes: (a) Uniform (conforming) mesh; (b) Mesh with 1–irregular elements; (c) Mesh with 3–irregular elements.

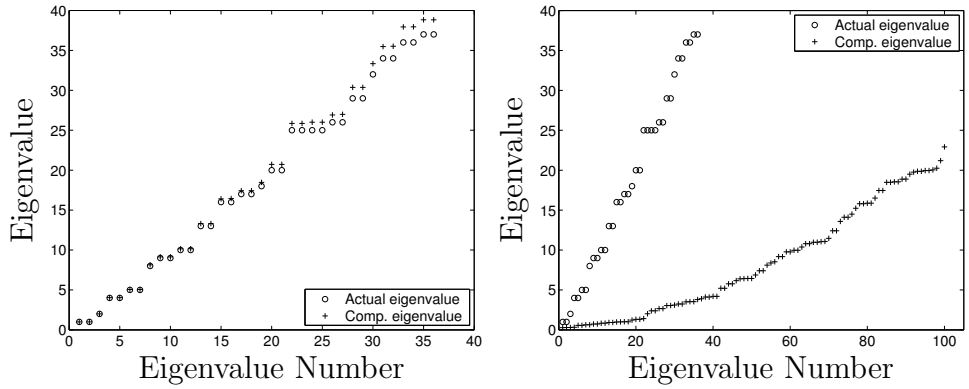

(a) (b)

Figure 2. Example 1. Lower part of the eigenspectrum computed using the SIP method with: (a) P_1 polynomials on a uniform triangular mesh; (b) Q_1 polynomials on a uniform square mesh.

computed using the SIP method based on employing both a uniform triangular mesh of the type shown in Figure 1(a) with piecewise discontinuous linear polynomials, as well as for a uniform square mesh with discontinuous Q_1 polynomials. Here, we observe that the SIP method produces an accurate representation of the eigenspectrum when triangular elements are employed. In contrast, when square elements with full Q_1 polynomials are used, spurious eigenvalues are generated which pollute the computed spectrum, as indeed expected (see Remark 4.5).

In Figure 3 we now present a comparison of the error in the eighth eigenvalue (exact value is 8), on each type of mesh employed, as well as the DG–norm $\|\cdot\|_{\mathbf{V}(h)}$ of the error in the eighth eigenvector, computed on uniform (conforming) meshes, with the square root of the number of degrees of freedom in the finite element space $\mathbf{V}_h$, for the SIP method. Here, we clearly observe that the error in the computed eigenvalue converges to zero, for each fixed ℓ, at the rate $\mathcal{O}(h^{2\ell})$ as the mesh is refined. We remark that this rate of con-

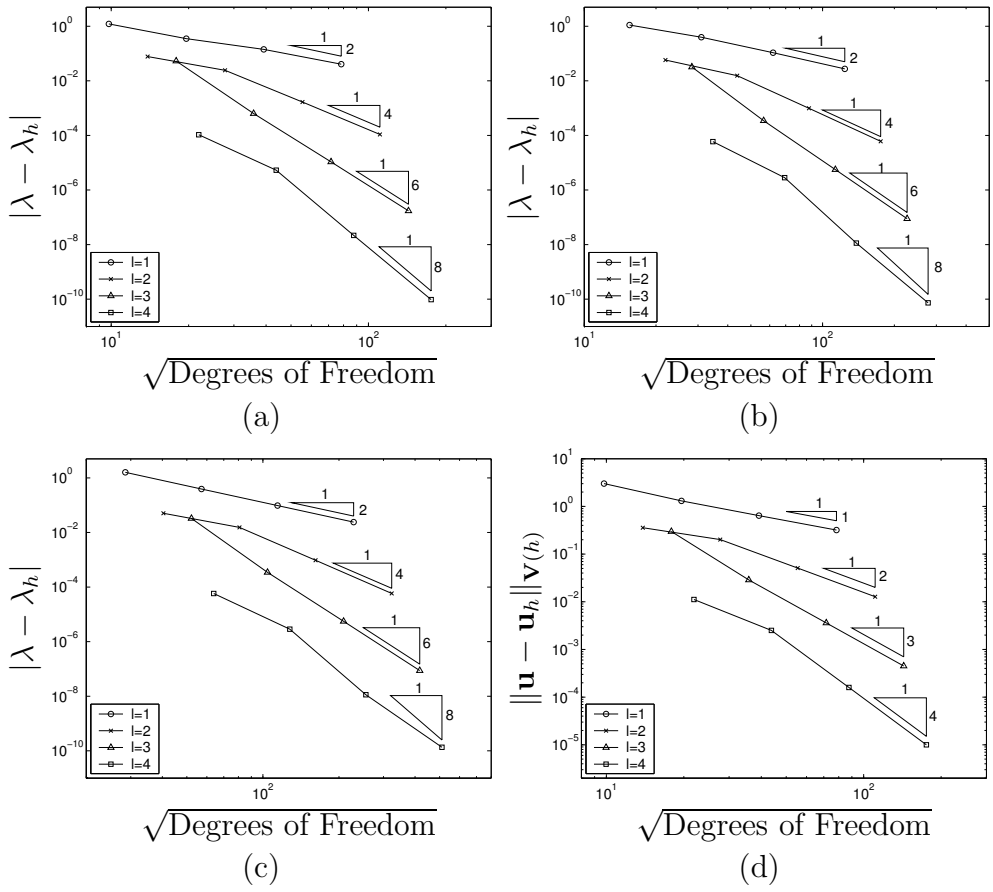

Figure 3. Example 1. SIP method: (a), (b) & (c) Error in the eighth eigenvalue computed on uniform triangular meshes, and meshes with 1– and 3–irregular elements, respectively; (d) Error in the eighth eigenfunction on uniform triangular meshes.

vergence is indeed in agreement with Theorem 4.3; moreover, we observe that the inclusion of hanging nodes in the underlying computational mesh does not lead to a degradation in the order of convergence of the SIP method. From Figure 3(d) we observe that the error in the computed eigenvector tends to zero at the optimal rate $\mathcal{O}(h^\ell)$, for each fixed ℓ, as h tends to zero on uniform triangular meshes, cf. Theorem 4.3. Analogous behaviour is also observed on meshes containing hanging nodes; for brevity, these results have been omitted.

We now turn our attention to the NIP method. In Figure 4 we plot the values of the first 36 eigenvalues computed based on employing each of the meshes depicted in Figure 1, after one uniform mesh refinement has been undertaken, as well as on an unstructured conforming triangular mesh, with $\ell = 1$. Here, we observe that for both the conforming meshes, cf. Figures 4(a) & (d), the imaginary part of the computed eigenvalues is very close to zero. Indeed, on the uniform mesh employed here, the computed eigenvalues are actually real (to machine precision), though on other meshes of this type, we have observed small imaginary parts. Moreover, on the unstructured mesh, some of the larger eigenvalues do indeed become complex. In contrast, the introduction

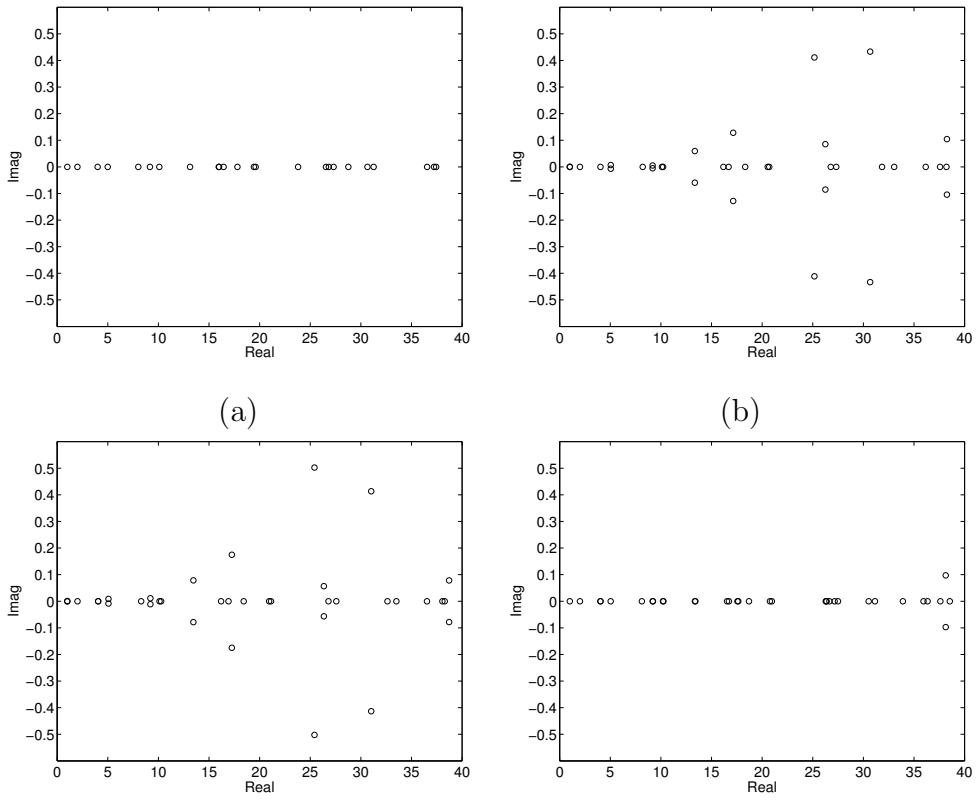

Figure 4. Example 1. First 36 eigenvalues computed using the NIP method with $\ell = 1$ on: (a) Uniform mesh with 64 elements; (b) 1–irregular mesh with 160 elements; (c) 3–irregular mesh with 544 elements; (d) Unstructured (conforming) triangular mesh with 104 elements.

of hanging nodes into the underlying computational mesh leads to a large number of complex eigenvalues with non-zero imaginary parts, cf. Figures 4(b) & (c).

In Figure 5 we present a comparison of the error in the eighth eigenvalue, on each type of mesh depicted in Figure 1, as well as the DG–norm $\|\cdot\|_{\mathbf{V}(h)}$ of the error in the eighth eigenvector, computed on the uniform (conforming) meshes, with the square root of the number of degrees of freedom, for the NIP method. In contrast to the SIP method, we now observe that the error in the computed eigenvalue converges to zero, for each fixed ℓ, at the rate $\mathcal{O}(h^{\ell})$ for even ℓ and $\mathcal{O}(h^{\ell+1})$ for odd ℓ, as the mesh is refined. The former rate of convergence is indeed in agreement with Theorem 4.3, in the case of conforming meshes, though for odd polynomial degrees the observed rate is a full power of h superior to the theoretical predictions. We remark that analogous behaviour for the NIP method was also observed in the recent article [1] where the numerical approximation of the Laplace eigenvalue problem was considered, as well as in [12] in the context of error estimation of linear target functionals

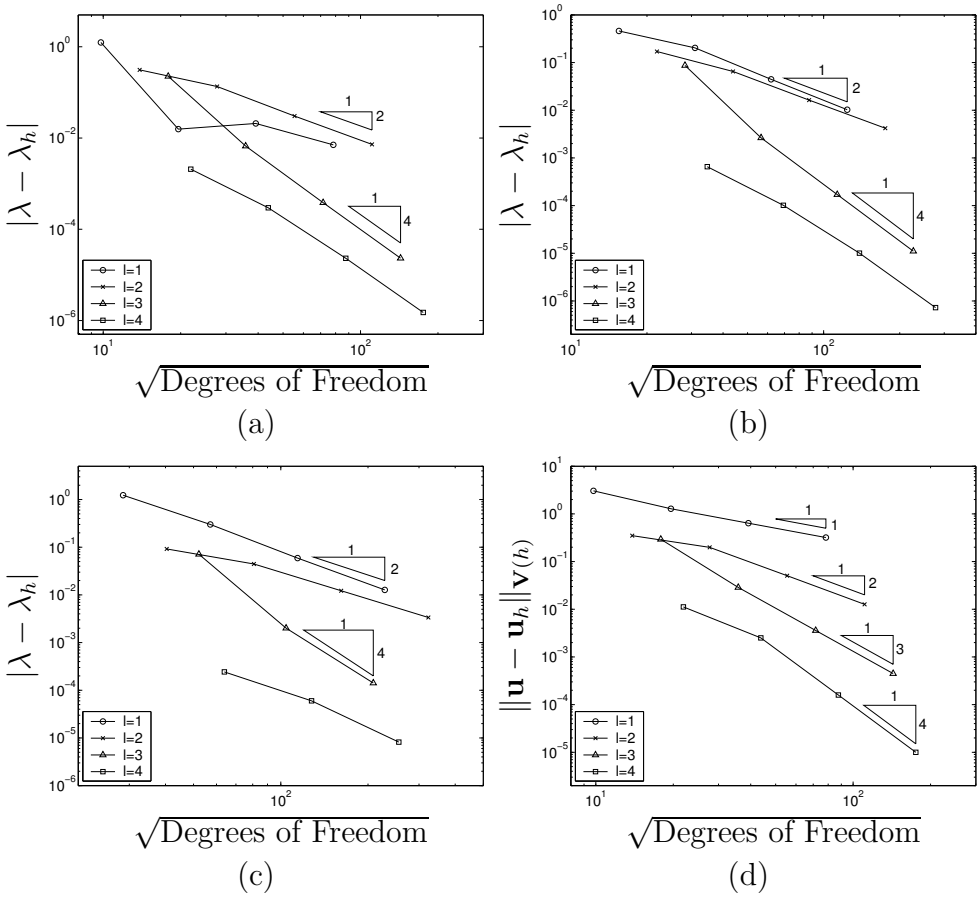

Figure 5. Example 1. NIP method: (a), (b) & (c) Error in the eighth eigenvalue computed on uniform triangular meshes, and meshes with 1– and 3–irregular elements, respectively; (d) Error in the eighth eigenfunction on uniform triangular meshes.

of the solutions to advection-diffusion-reaction problems. However, we note that the order of convergence of the error in the computed eigenvector is still optimal: here, we observe that the error decays to zero at the rate $\mathcal{O}(h^\ell)$, for each fixed ℓ, as h tends to zero.

In Table 1 we show the first 8 eigenvalues computed using both DG methods on a sequence of uniform triangular meshes, cf. Figure 1(a), for $\ell = 1$. Here, we observe that for low-order elements, the NIP method is actually more accurate than the SIP method; though given the superior rate of convergence of the SIP method for higher-order polynomials, the NIP method is in general inferior.

Finally, before we end this section, we now return to the issue concerning the necessity of the assumption concerning the conformity of the underlying mesh, cf. Theorem 4.3. The numerical experiments presented so far in this section based on employing the 1– and 3–irregular meshes depicted in Figures 1(b) & (c), respectively, indicate that the computed eigenspectrum does not contain any spurious modes. However, let us now consider more general non-conforming meshes, where the hanging nodes are not uniformly spaced along

Table 1
Example 1. Approximation of the first 8 eigenvalues using the SIP and NIP methods, with $\ell = 1$ on uniform triangular meshes.

Actual	SIP			NIP		
	$h = \pi/2$	$h = \pi/4$	$h = \pi/8$	$h = \pi/2$	$h = \pi/4$	$h = \pi/8$
1	1.0141	1.0062	1.0018	1.0045	1.0023	1.0007
1	1.0141	1.0062	1.0018	1.0045	1.0023	1.0007
2	2.0042	2.0186	2.0066	1.9757	2.0051	2.0024
4	3.9607	4.1121	4.0342	3.6772	4.0003	4.0032
4	4.0534	4.1128	4.0342	3.7268	4.0009	4.0032
5	4.6110	5.1345	5.0490	4.3852	4.9943	5.0061
5	4.6110	5.1345	5.0490	4.3852	4.9943	5.0061
8	6.7851	8.3525	8.1426	6.7561	8.0157	8.0209

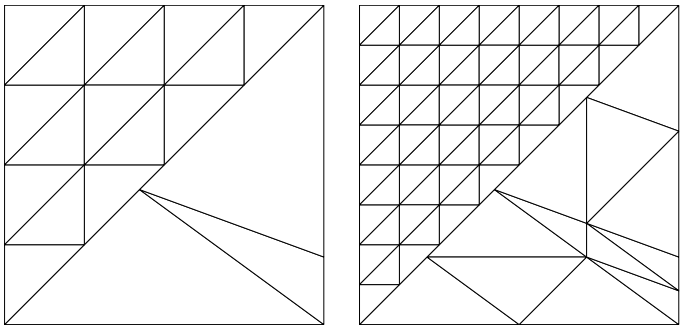

(a) (b)

Figure 6. Example 1. General non-conforming triangular meshes.

a given edge. To this end, we consider computing the eigenvalues on the two meshes shown in Figure 6 using the SIP method. In Figure 7 we show the lower part of the eigenspectrum computed on the mesh depicted in Figure 6(a). The first thing we notice is that there is some pollution of the eigenvalues close to zero. Secondly, we notice the generation of spurious eigenvalues; indeed, from Figure 7(b), we see that the eigenvalue with value 4 appears with multiplicity 3, rather than 2, when order 8 polynomials are employed, though for $\ell = 6$, the correct multiplicity is observed. Similar behaviour is also observed in Table 2 when the mesh shown in Figure 6(b) is employed. Indeed, in this case we see that as the polynomial degree is increased, there appears to be a greater number of small, but not zero, eigenvalues being generated. Again, as before eigenvalues with the incorrect multiplicity are also generated.

In summary, on the basis of these numerical experiments, it would appear that meshes with regularly spaced hanging nodes, cf. Figure 1, give rise to

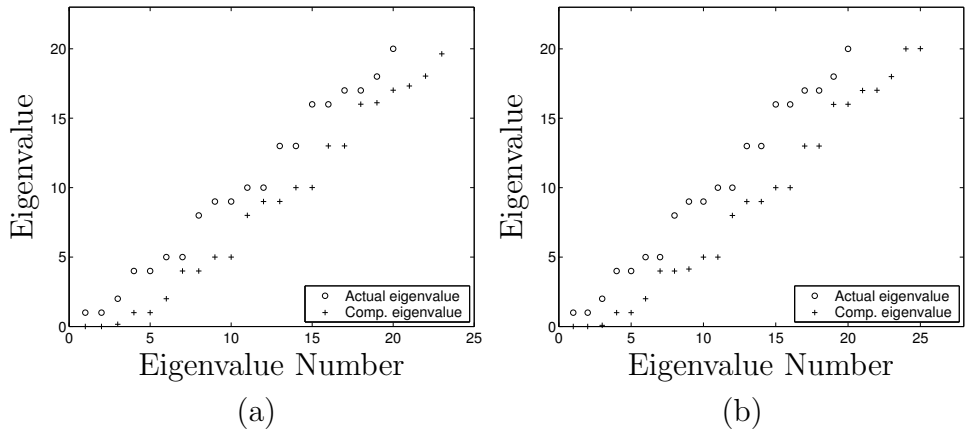

Figure 7. Example 1. Lower part of the eigenspectrum computed using the SIP method on the mesh shown in Figure 6(a): (a) $\ell = 6$; (b) $\ell = 8$.

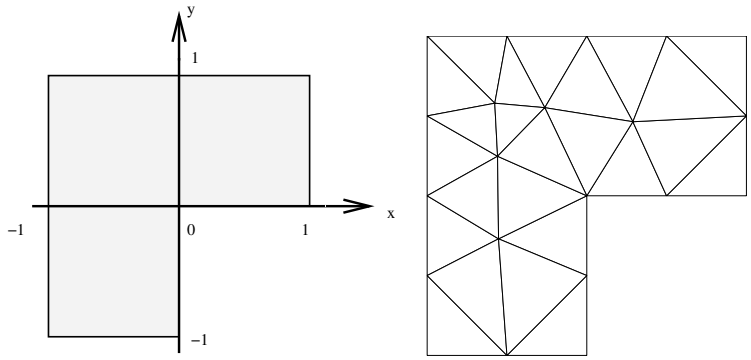

Figure 8. Example 2. (a) Problem domain; (b) Initial unstructured triangular mesh.

an accurate spurious-free approximation to the eigenspectrum of the underlying Maxwell operator, while more general non-conforming meshes lead to a pollution of the computed eigenvalues.

5.2 Example 2

In this second example we consider the computation of the eigenvalues of the Maxwell operator in a non-convex domain. To this end, we let $\Omega = (-1,1)^2 \setminus [0,1) \times (-1,0]$, cf. Figure 8(a), and select $\varepsilon = I$ and $\mu = I$. The first 5 eigenvalues are: 1.47562182408, 3.53403136678, π^2, π^2, and 11.3894793979, cf. [8]. We note that the first and fifth Maxwell eigenvectors have a strong unbounded singularity at the re-entrant corner, the second one belongs to $H^1(\Omega)^2$, while the third and fourth ones are analytic.

In Figure 9 we plot the error in the computed values of the first, second, and third eigenvalues for both the SIP and NIP methods as the mesh is refined for $\ell = 1, 2, 3, 4$. Here, the meshes employed are based on uniform refinements of the unstructured (conforming) triangular mesh shown in Figure 8(b). For the

Table 2
Example 1. Approximation of the first 8 eigenvalues using the SIP method on the non-conforming triangular mesh depicted in Figure 6(b).

			ℓ		
Actual	1	2	3	4	5
-	-	-	-	2.3252e-8	1.3693e-8
-	-	-	-	1.6285e-7	1.1637e-5
-	-	-	2.9670e-6	1.9828e-6	8.5029e-5
-	-	2.4294e-4	2.0809e-5	7.9350e-4	7.0652e-4
-	7.1646e-3	1.7448e-3	2.2217e-4	5.9337e-3	8.5626e-3
-	5.4994e-2	1.5389e-2	3.6357e-2	4.0764e-2	3.8575e-2
-	0.32229	0.86222	0.23450	0.34050	0.31105
1	1.0097	1.0001	1.0000	1.0000	1.0000
1	1.0158	1.0003	1.0000	1.0000	1.0000
-	-	-	1.0841	1.2822	-
2	2.0329	2.0023	2.0001	2.0000	2.0000
4	3.9664	3.5380	4.0003	4.0000	4.0000
4	4.0920	4.0188	4.0015	4.0000	4.0000
-	4.3188	4.0271	-	4.1944	4.1061
5	4.8189	5.0295	5.0014	5.0000	5.0000
5	5.1519	5.0481	5.0039	5.0001	5.0000
8	7.4832	8.0490	7.8329	8.0001	8.0000
-	8.3266	8.0625	8.0153	-	-

first eigenvalue, we observe that both methods converge at the rate $\mathcal{O}(h^{1.33})$ as h tends to zero, for each polynomial degree employed. For the second eigenvalue we observe that the error in the computed eigenvalue tends to zero at the rate $\mathcal{O}(h^{\min(2\ell,2.67)})$ as the mesh is refined for the SIP method. In contrast, when the NIP method is employed, for $\ell = 2$ the error in the computed eigenvalue using this non-hermitian method decays to zero at the inferior rate of $\mathcal{O}(h^2)$, as h tends to zero. For the third eigenvalue, whose eigenvector is analytic, we see analogous behaviour to that observed in Example 1: for the SIP method the error decays to zero at the optimal rate $\mathcal{O}(h^{2\ell})$, as h tends to zero; in contrast, a rate of $\mathcal{O}(h^{\ell})$ is observed for even polynomials, and a rate of $\mathcal{O}(h^{\ell+1})$ is attained for odd polynomials, as the mesh is refined, when the NIP method is employed.

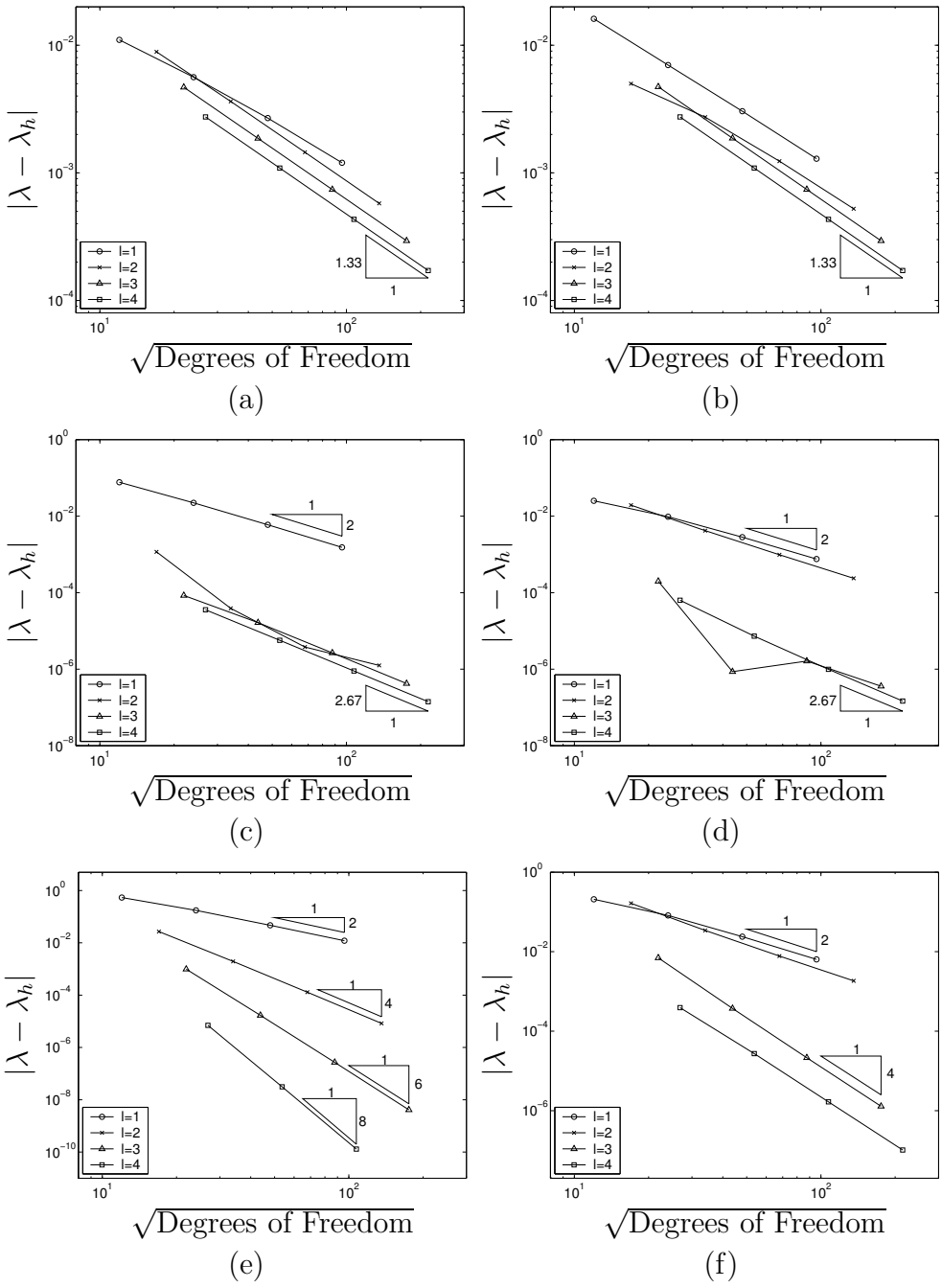

Figure 9. Example 2. (a) & (b), (c) & (d), and (e) & (f) Error in the first, second, and third eigenvalues, respectively, computed on quasi-uniform unstructured triangular meshes; Left: SIP; Right: NIP.

5.3 Example 3

In this final example we consider a problem with discontinuous coefficients. To this end, we let $\Omega = (-1, 1)^2$ with $\mu = I$ and $\varepsilon = \varepsilon_r I$, where ε_r is a piecewise constant positive function. Here, we select $\varepsilon_r = 0.1$ in the first and third quad-

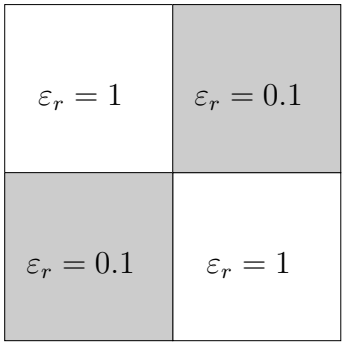

Figure 10. Example 3. Problem domain and electric permittivity.

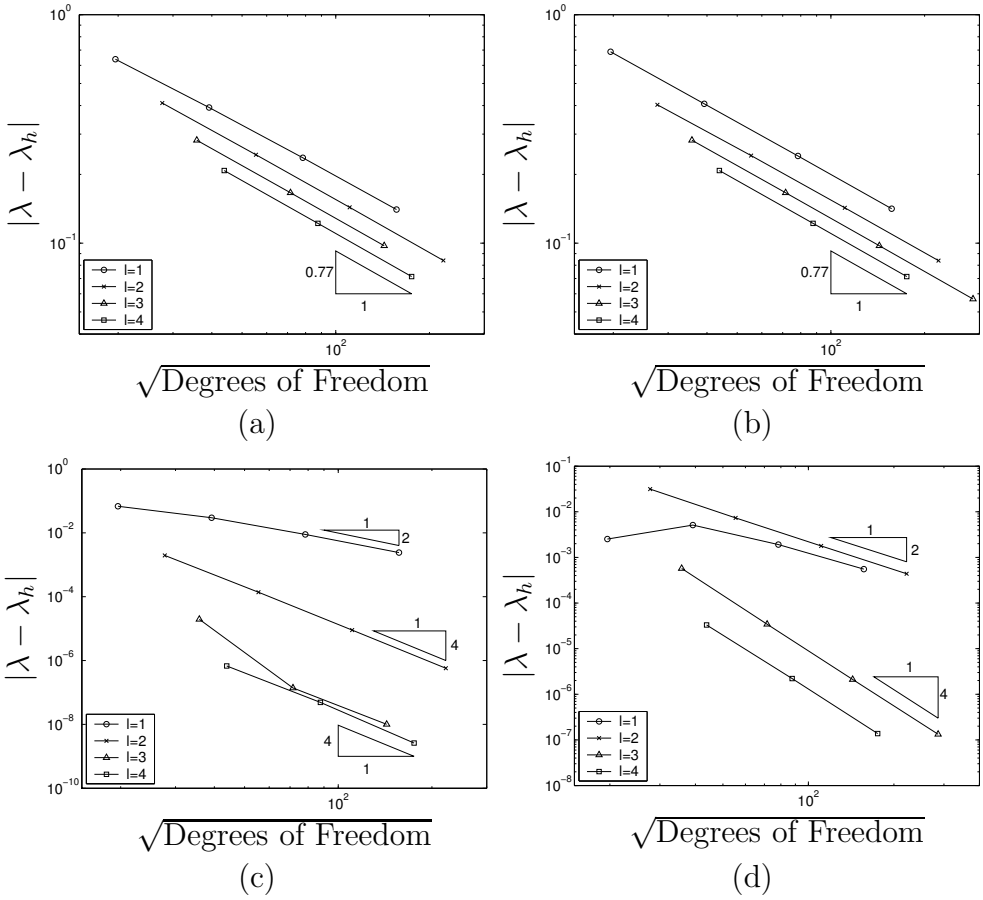

Figure 11. Example 3. (a) & (b) and (c) & (d) Error in the second and third eigenvalues, respectively, computed on uniform triangular meshes; Left: SIP; Right: NIP.

rants of Ω and $\varepsilon_r = 1$ elsewhere, cf. Figure 10. This choice of (discontinuous) material coefficients leads to the generation of singularities in the underlying eigenvectors. In particular, the strongest singularity behaves like $r^{-0.6}$, as r tends to zero, where r measures the distance from the origin; we remark the eigenfunction corresponding to the second eigenvalue (approximate value 6.250332186603, cf. [8]) contains such a singularity, cf. [8]. From Figures 11(a)

& (b), we observe that both the SIP and NIP methods, respectively, lead to a slightly superior rate of convergence of order $\mathcal{O}(h^{0.77})$ as the mesh is uniformly refined; here, uniform triangular meshes of the type depicted in Figure 1(a) have been employed. Finally, in Figures 11(c) & (d) we plot the computed error in the third eigenvalue (approximate value 7.037074196012, cf. [8]) against the square root of the number of degrees of freedom in $\mathbf{V}_h$ for both DG methods. Here, for the SIP method we observe a rate of convergence of $\mathcal{O}(h^{\min(2\ell,4)})$, as h tends to zero. As noted previously, the NIP method gives rise to suboptimal convergence; here, for $\ell = 2$ only $\mathcal{O}(h^2)$ convergence is attained as the mesh is uniformly refined.

References

[1] P.F. Antonietti, A. Buffa, and I. Perugia. Discontinuous Galerkin approximation of the Laplace eigenproblem. *Comput. Methods Appl. Mech. Engrg.* to appear.

[2] D.N. Arnold. An interior penalty finite element method with discontinuous elements. *SIAM J. Numer. Anal.*, 19:742–760, 1982.

[3] D.N. Arnold, F. Brezzi, B. Cockburn, and L.D. Marini. Unified analysis of discontinuous Galerkin methods for elliptic problems. *SIAM J. Numer. Anal.*, 39:1749–1779, 2001.

[4] D. Boffi. Fortin operator and discrete compactness for edge elements. *Numer. Math.*, 87:229–246, 2000.

[5] A. Buffa and I. Perugia. Discontinuous Galerkin approximation of the Maxwell eigenproblem. Technical Report 24-PV, IMATI-CNR, Pavia, Italy, 2005. `http://www.imati.cnr.it/~annalisa/PS/maxwell.pdf`.

[6] S. Caorsi, P. Fernandes, and M. Raffetto. On the convergence of Galerkin finite element approximations of electromagnetic eigenproblems. *SIAM J. Numer. Anal.*, 38:580–607, 2000.

[7] M. Costabel, M. Dauge, and S. Nicaise. Singularities of Maxwell interface problems. *Modél. Math. Anal. Numér.*, 33:627–649, 1999.

[8] M. Dauge. Computations for Maxwell equations for the approximation of highly singular solutions
`http://perso.univ-rennes1.fr/monique.dauge/benchmax.html`.

[9] C. Dawson, S. Sun, and M.F. Wheeler. Compatible algorithms for coupled flow and transport. *Comput. Methods Appl. Mech. Engrg.*, 193:2565–2580, 2004.

[10] J. Descloux, N. Nassif, and J. Rappaz. On spectral approximation Part 1. The problem of convergence. *RAIRO Modél. Math. Anal. Numér.*, 12:97–112, 1978.

[11] J. Descloux, N. Nassif, and J. Rappaz. On spectral approximation Part 2. Error estimates for the Galerkin method convergence. *RAIRO Modél. Math. Anal. Numér.*, 12:113–119, 1978.

[12] K. Harriman, P. Houston, B. Senior, and E. Süli. *hp*-version discontinuous Galerkin methods with interior penalty for partial differential equations with nonnegative characteristic form. In C.-W. Shu, T. Tang, and S.-Y. Cheng, editors, *Recent Advances in Scientific Computing and Partial Differential Equations*, volume 330 of *Contemporary Mathematics*, pages 89–119. AMS, 2003.

[13] J.S. Hesthaven and T. Warburton. High order nodal discontinuous Galerkin methods for the Maxwell eigenvalue problem. *Philos. Trans. R. Soc. Lond. Ser. A Math. Phys. Eng. Sci.*, 362:493–524, 2004.

[14] P. Houston, I. Perugia, A. Schneebeli, and D. Schötzau. Interior penalty method for the indefinite time-harmonic Maxwell equations. *Numer. Math.*, 100:485–518, 2005.

[15] P. Houston, I. Perugia, and D. Schötzau. *hp*-DGFEM for Maxwell's equations. In F. Brezzi, A. Buffa, S. Corsaro, and A. Murli, editors, *Numerical Mathematics and Advanced Applications ENUMATH 2001*, pages 785–794. Springer-Verlag, 2003.

[16] P. Houston, I. Perugia, and D. Schötzau. Mixed discontinuous Galerkin approximation of the Maxwell operator: Non-stabilized formulation. *J. Sci. Comp.*, 22:325–356, 2005.

[17] T. Kato. *Perturbation theory of linear operators*. Springer-Verlag, 1966.

[18] P. Monk. *Finite element methods for Maxwell's equations*. Oxford University Press, New York, 2003.

[19] J.C. Nédélec. Mixed finite elements in $\mathbb{R}^3$. *Numer. Math.*, 35:315–341, 1980.

[20] B. Rivière, M.F. Wheeler, and V. Girault. Improved energy estimates for interior penalty, constrained and discontinuous Galerkin methods for elliptic problems, Part I. *Computational Geosciences*, 3:337–360, 1999.

[21] T. Warburton and M. Embree. The role of the penalty in the local discontinuous Galerkin method for maxwell's eigenvalue problem. *Comput. Methods Appl. Mech. Engrg.* to appear.